Earthquakes and Structures, *Vol. 8, No. 4 (2015) 859-887*
DOI: http://dx.doi.org/10.12989/eas.2015.8.4.859

Operational modal analysis of a long-span suspension bridge under different earthquake events

Yi-Qing Ni[1a], Feng-Liang Zhang[*1,2], Yun-Xia Xia[1b] and Siu-Kui Au[3c]

[1]Department of Civil and Environmental Engineering, The Hong Kong Polytechnic University, Hung Hom, Kowloon, Hong Kong
[2]Research Institute of Structural Engineering and Disaster Reduction, Tongji University, 1239 Siping Road, Shanghai, China
[3]Institute for Risk and Uncertainty and Centre for Engineering Dynamics, University of Liverpool, The Quadrangle, Brownlow HillL69 3GH, United Kingdom

(Received April 21, 2014, Revised October 4, 2014, Accepted October 8, 2014)

Abstract. Structural health monitoring (SHM) has gained in popularity in recent years since it can assess the performance and condition of instrumented structures in real time and provide valuable information to the asset's manager and owner. Operational modal analysis plays an important role in SHM and it involves the determination of natural frequencies, damping ratios and mode shapes of a constructed structure based on measured dynamic data. This paper presents the operational modal analysis and seismic response characterization of the Tsing Ma Suspension Bridge of 2,160 m long subjected to different earthquake events. Three kinds of events, i.e., short-distance, middle-distance and long-distance earthquakes are taken into account. A fast Bayesian modal identification method is used to carry out the operational modal analysis. The modal properties of the bridge are identified and compared by use of the field monitoring data acquired before and after the earthquake for each type of the events. Research emphasis is given on identifying the predominant modes of the seismic responses in the deck during short-distance, middle-distance and long-distance earthquakes, respectively, and characterizing the response pattern of various structural portions (deck, towers, main cables, etc.) under different types of earthquakes. Since the bridge is over 2,000 m long, the seismic wave would arrive at the tower/anchorage basements of the two side spans at different time instants. The behaviors of structural dynamic responses on the Tsing Yi side span and on the Ma Wan side span under each type of the earthquake events are compared. The results obtained from this study would be beneficial to the seismic design of future long-span bridges to be built around Hong Kong (e.g., the Hong Kong-Zhuhai-Macau Bridge).

Keywords: long-span bridge; earthquake excitation; operational modal analysis; identification of predominant modes; structural condition assessment

1. Introduction

∗Corresponding author, Assistant Professor, E-mail: zhangfengliang6@gmail.com
[a]Professor, E-mail: ceyqni@polyu.edu.hk
[b]Ph.D. Student, E-mail: yunxia.xia@connect.polyu.hk
[c]Professor, E-mail: Siu-Kui.Au@liverpool.ac.uk

http://www.techno-press.org/?journal=eas&subpage=7 ISSN: 2092-7614 (Print), 2092-7622 (Online)

With the development of economy and modern construction technology, more and more large-scale structures such as long suspension or cable-stayed bridges, super-tall buildings have been or are being built (Brownjohn *et al.* 2005, Ni *et al.* 2011). Meanwhile, structural health monitoring (SHM) has attracted enormous attention for the assessment of structural performance. SHM systems have been instrumented in important civil structures and infrastructure systems in different countries around the world. Up to now, more than 50 bridges including suspension bridges, cable-stayed bridges, arch bridges and truss bridges in China have been instrumented with long-term SHM systems (Ko and Ni 2005, Ou and Li 2009). The SHM systems can provide real-time information on structural performance under in-service condition and during extreme events and help engineers to evaluate the structural integrity and safety after rare events or long-term service. Furthermore, the data collected during typhoons and earthquakes can be used to calibrate/validate the parameters and criteria used in wind- and earthquake-resistant design, which are also highly valuable for instructing the design of similar structures to be built in the same region (Ko and Ni 2005, Ou and Li 2009, Ivanovic *et al.* 2000, Ni *et al.* 2009, Au *et al.* 2013).

The characterization of dynamic properties of structures is essential for investigating their response subjected to extreme loads, e.g., earthquakes. The dynamic properties of a structure can be characterized by its modal properties such as modal frequencies, modal damping ratios, mode shapes, and modal masses. For instrumented structures, accelerometers are usually installed to measure the structural dynamic responses in real time. These responses can be used to determine the modal parameters of the monitored structure by performing operational modal analysis, which is usually the first step for the subsequent model updating, vibration-based damage detection and structural vibration control, etc.

Considerable studies have been made to investigate the modal parameter identification under earthquake recordings. Beck and Jennings (1980) developed an algorithm to determine the optimal estimates of the modal parameters of structures subjected to earthquake excitation and applied this method to study the structural behavior of a multi-story building using records from the 1971 San Fernando earthquake in California. Loh and Lin (1996) presented the dynamic characteristics of a seven-story reinforced concrete building during four strong motion earthquakes. Loh and Lee (1997) assessed the dynamic characteristics from both weak and strong excitations by monitoring a bridge. It was found that the damping ratios of pier and girder would increase subjected to different levels of seismic excitations. Arici and Mosalam (2003) applied parametric and non-parametric system identification (SI) methods to study the response of seven bridge systems in California under several earthquake excitations. The change of the modal frequencies and damping was identified during earthquakes. Smyth *et al.* (2003) presented the work on the system identification of a suspension bridge using earthquake records. Some difficulties in identifying the structural dynamic behavior of a long span bridge were illustrated and discussed. Siringoringo and Fujino (2006) focused on the analysis of strong motion data collected from Yokohama-Bay Bridge in Japan during six earthquakes. The global behavior of the bridge was captured by investigating the modal parameters, while the local behavior of some structural components was also explained by system identification. Subsequently, Michel *et al.* (2010) carried out an investigation on the structural response of the Grenoble City Hall building in France based on the weak earthquake records. About 2% variation in the natural frequencies was observed by comparing the modal parameters identified from ambient vibrations and from weak earthquakes. Todorovska and Trifunac (2008) analyzed the response data of a 7-storey hotel from 11 earthquakes over a period of 24 years. It was found that it would be a powerful tool for structural health monitoring to monitor the changes of fundamental fixed-base frequency of the building before, during, and after excitation by strong earthquake motions. Ulusoy *et al.* (2011) performed the system identification of a 4-story building using multiple data sets of earthquake response. It was demonstrated that the response of the building was amplitude-dependent. This finding makes it possible to assess the consistency of the building response to future earthquakes. Gomez *et al*. (2013) presented their study on the variation of modal parameters of a three-span curved highway bridge using the acceleration responses measured in six earthquakes from 2005 to 2010. It was shown that the identified frequencies and damping ratios were dependent on the earthquake intensity.

The change in modal parameters is an indicator of the change of structural behavior or structural damage. However, global modal change is usually not obvious and if the identified result is not accurate enough, it is difficult to quantify the modal change with fidelity. Therefore, uncertainty quantification is becoming increasingly important in modern engineering problems (Papadimitriou *et al.* 2001, Yuen and Katafygiotis 2003, Beck 2010, Au and Zhang 2011). The fast Bayesian FFT method is a frequency-domain method and has attracted increasing attention in recent years (Au 2011, Zhang and Au 2013, Au 2012a, b). A salient merit of the Bayesian method is that it provides a rigorous means for identifying the most probable value (MPV) and quantifying the posterior uncertainty of the identified parameters consistent with modeling assumptions (Beck 2010).

The Tsing Ma Bridge (TMB) spanning between the Tsing Yi Island and the Ma Wan Island in Hong Kong was built in 1997 and it is one of the longest suspension bridges in the world. In the past two decades, there were numerous earthquakes recorded by the Hong Kong Observatory. According to the distance between the epicenters and Hong Kong, we can mainly classify the earthquakes into three kinds, i.e., short-, middle- and long-distance events. After completing construction in 1997, the TMB has been instrumented with a sophisticated long-term SHM system (Wong 2004, Wong and Ni 2011). The system has captured the structural responses of TMB during a number of earthquakes. This paper presents an investigation on the operational modal analysis of TMB using the fast Bayesian FFT method under different types of earthquakes and characterizing the seismic response pattern of different structural portions (deck, towers, main cables, etc.). Three representative earthquake events, i.e., Wenchuan Earthquake (long-distance earthquake), Taiwan Earthquake (middle-distance earthquake) and Heyuan Earthquake (short-distance earthquake) are chosen for this study. Since the bridge is over 2,000 m long, the seismic wave would arrive at the tower/anchorage basements of the Tsing Yi side span and the Ma Wan side span of the bridge at different time instants. In recognizing this, a comparative study is made on the behaviors of the structural seismic responses on the two side spans (in the vicinity of the Tsing Yi tower and the Ma Wan tower) under each type of the earthquake events.

2. Tsing Ma Bridge (TMB)

The TMB is a suspension bridge with an overall length of 2,160 m and a main span of 1,377 m as shown in Fig. 1, which carries two railway tracks and two emergency highway lanes on its lower deck, and six lanes of highway traffic on its upper deck. The steel bridge deck is a continuous structure between anchorages with 96 deck units connected, where each unit is 18 m long, 41 m wide and 7.5 m high. The two towers (Tsing Yi tower and Ma Wan tower) are made of pre-stressed reinforced concrete with a height of 206 m each. The main span deck and the Ma Wan side span deck are suspended by hangers to the two main cables at intervals of 18 m. Instead, the Tsing Yi side span deck is supported by three concrete piers spaced at 72 m centers. To investigate

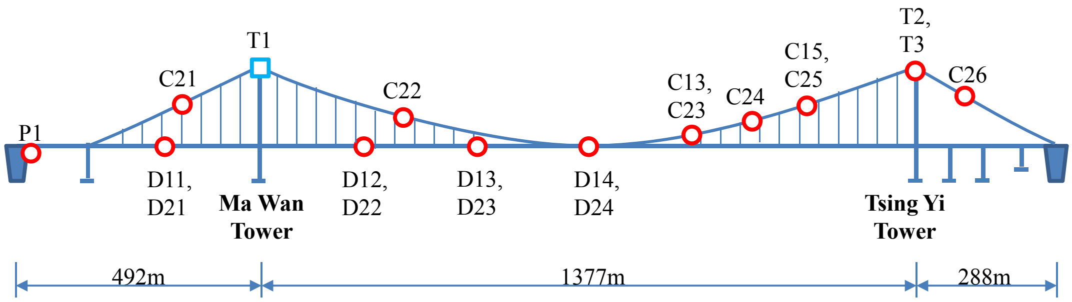

Fig. 1 Sensor deployment on Tsing Ma Bridge

the feasibility of using changes in measured dynamic characteristics for the assessment of structural performance, a three-dimensional finite element model of the bridge has been formulated (Ni *et al*. 1999, Wang *et al*. 2000). This model has been validated through a comparison between the computed and measured modal parameters, i.e., natural frequencies and mode shapes. For the first four lateral, vertical and torsional modes (12 global modes in total), the maximum relative difference between the computed and measured natural frequencies is 6.97% (Wang *et al.* 2000).

The TMB has been permanently instrumented with about 300 sensors of different types for monitoring the structural performance and evaluating the health condition of the bridge. These sensors include accelerometers, displacement transducers, anemometers, strain gauges, level sensors, temperature sensors, GPS receivers, and a weigh-in-motion system. Among those, accelerometers were installed to collect the structural dynamic responses under ambient vibration conditions and during extreme events (typhoons, earthquakes, ship collisions, etc.). The detailed positions of the accelerometers are illustrated in Fig. 1. The circles in the figure indicate the deployment locations of sensors. The letters 'D', 'C', 'T' and 'P' denote the sensors installed on the deck, cables, towers, and anchorage, respectively. The numbers after 'D' and 'C' are the code of sensors, where the first number indicates which side of a bridge section the sensor is located, i.e., '1' represents the sensor situated at the right side of a bridge section (view from the Ma Wan side to the Tsing Yi side) while '2' represents the sensor situated at the left side of a bridge section; the second number indicates the location code. For example, 'D12' refers to the right side of a section and the second location on the deck; 'C24' refers to the left side of a section and the fourth location on the cables.

There are 8 uniaxial accelerometers (vertical direction), 9 bi-axial accelerometers (lateral and vertical directions), 2 tri-axial accelerometers (longitudinal, lateral and vertical directions) installed on TMB with a total number of 32 channels. Among them, twelve channels are instrumented on the deck, including four uniaxial accelerometers instrumented at the right side of four deck sections (D11, D12, D13 and D14) and four bi-axial accelerometers at the left side of the same deck sections (D21, D22, D23 and D24). The vertical sensors at the two sides are symmetric. On the main span, six locations from the middle to the Ma Wan tower are measured. The other two locations are situated on the Ma Wan side span.

Fifteen channels are instrumented on the main cables for the measurement at six locations including one location on the left main cable over the Ma Wan side span (C21, bi-axial sensor), one location on the left main cable over the Tsing Yi side span (C26, bi-axial sensor), and four locations on the left and right main cables over the main span (C22: tri-axial, C13: uniaxial, C23:

bi-axial, C24: bi-axial, C15: uniaxial, and C25: bi-axial). The number after 'T' and 'P' also indicates the numbering of sensor. Note that two uniaxial accelerometers are instrumented on the top of the Tsing Yi tower (T2 and T3), while one GPS receiver for displacement measurement is installed on the top of the Ma Wan tower (T1). At the anchorage of the Ma Wan side span, a tri-axial sensor is installed (P1).

3. Earthquake events

The structural response data employed in the present study were acquired during three earthquake events, namely, Wenchuan Earthquake, Taiwan Earthquake, Heyuan Earthquake.

3.1 Wenchuan Earthquake: a long-distance earthquake

The Wenchuan Earthquake struck in Sichuan Province, China, at 2:28:04 pm of May 12, 2008. The earthquake with the magnitude of 8.0 is one of the largest earthquakes in China in the past few decades, during which about 70,000 persons were killed, 18,000 missing, and 375,000 injured. The quake was felt in the majority of the territory of China. According to the data from China Earthquake Network Center (CENC) (http://www.csndmc.ac.cn/newweb/index.jsp), the focal depth is about 14 km and it belongs to shallow-focus earthquake. The distance between Hong Kong and Wenchuan city is about 1,440 km. From the record of Hong Kong Observatory (http://www.weather.gov.hk/contente.htm), more than 30 persons reported that they had the feeling about the earthquake. This event is considered as a long-distance earthquake.

When the earthquake happened, the accelerometers and displacement sensors on the bridge captured the structural dynamic responses. According to the difference in sampling frequency, the sensors are classified as two kinds, i.e., fast and slow. The ones instrumented on the towers are slow sensors with a sampling frequency of 2.56 Hz, while the others are all fast sensors with a sampling frequency of 51.2 Hz. Since the first several modes of the bridge are less than 1 Hz, the sampling frequency is high enough for the operational modal analysis later on.

3.2 Taiwan Earthquake: a middle-distance earthquake

At 8:26:18.8 pm of December 26, 2006, an earthquake with the magnitude of 7.2 occurred beneath the sea near Southern Taiwan, which is about 660 km away from Hong Kong. According to the data from CENC, the focal depth is about 15 km and it also belongs to shallow-focus earthquake. This is a severe earthquake in Taiwan. Since the epicenter is about 90 km away from Kaohsiung city, Taiwan, there was no much casualty for the persons. Persons in different cities in Taiwan and in Chinese southeast coastal region felt the quake. From the record of Hong Kong Observatory, more than 300 persons reported that they had the feeling about the earthquake. This event is considered as a middle-distance earthquake.

3.3 Heyuan Earthquake: a short-distance earthquake

The earthquake occurred at 11:34:12.1 am of February 22, 2013 in Heyuan, Guangdong Province, China, with the magnitude of 4.8, which is much smaller than the former two in magnitude. According to the data from CENC, the focal depth is about 15 km and it belongs to shallow-focus earthquake. The distance between Heyuan city and Hong Kong is about 180 km, and therefore the event is considered as a short-distance earthquake. Since a new online reporting system about felt earth tremors was adopted, when the earthquake happened, there were more than 5,000 persons reporting that they had felt the earthquake. Since TMB had not suffered from any strong earthquake occurring in Guangdong region before, this one is a relatively large event around Hong Kong.

4. Methodology for operational modal analysis

The acceleration response data acquired during the three earthquake events are used to identify the modal properties of the bridge. Usually, an earthquake strike lasts only a short duration. Considering the fact that the natural frequency of the first mode of the bridge is about 0.07 Hz, a 30-minute time window is set to yield sufficient amount of data for a reliable estimate of the modal parameters. By taking the time instant at which the earthquake happened as a breakpoint, the 30-minute data before this time instant is named as Data 1; the 30-minute data since this time instant is named as Data 2; and the data from 31 minutes to 60 minutes after this time instant is named Data 3. These data for each earthquake will be investigated later.

4.1 Bayesian modal identification

The Fast Bayesian FFT method is used to identify the modal properties with each set of data in 30-minute time window. In addition to the most probable value (MPV), the Bayesian identification procedures also provide a rigorous quantitative assessment of the uncertainties associated with the modal parameters given the available data. This is one major merit of the Bayesian identification methods over non-Bayesian methods. The theory is outlined in the following. The original formulation can be found in (Yuen and Katafygiotis 2003). For the recently developed fast algorithms that allow practical implementation, refer to Au (2011), Zhang and Au (2013), Au (2012a, b).

The digitally acquired acceleration data can be assumed to consist of the structural dynamic response and prediction error

$$\hat{\ddot{\mathbf{x}}}_j = \ddot{\mathbf{x}}_j + \mathbf{e}_j \tag{1}$$

where $\ddot{\mathbf{x}}_j \in R^n$ and $\mathbf{e}_j \in R^n$ (j=1,2,…,N) are the acceleration response of a structure and prediction error, respectively; n denotes the number of measured degrees of freedom (DOFs); N denotes the number of sampling points. The FFT of $\hat{\ddot{\mathbf{x}}}_j$ is defined as

$$\mathcal{F}_k = \sqrt{\frac{2\Delta t}{N}} \sum_{j=1}^{N} \hat{\ddot{\mathbf{x}}}_j \exp[-2\pi \mathbf{i} \frac{(k-1)(j-1)}{N}] \tag{2}$$

where $\mathbf{i}^2=-1$; k=1,…,N_q with N_q=int[N/2]+1, int[.] is the integer part of its argument; N_q denotes the index that corresponds to the Nyquist frequency; Δt denotes the sampling interval.

Let $\boldsymbol{\theta}$ denote the modal parameters to be identified, which include natural frequencies, damping ratios, mode shapes, power spectral density (PSD) matrix of modal forces, and PSD of prediction error. Let $\mathbf{Z}_k = [\mathrm{Re}\mathcal{F}_k; \mathrm{Im}\mathcal{F}_k] \in R^{2n}$ denote an augmented vector of the real and imaginary part of $\mathcal{F}_k$. In practice, only the FFT data confined to a selected frequency band dominated by the target modes are used for modal identification. Such collection is denoted by $\{\mathbf{Z}_k\}$. Based on Bayes' Theorem, the posterior probability density function (PDF) of $\boldsymbol{\theta}$ given the data is expressed by

$$p(\boldsymbol{\theta} \,|\, \{\mathbf{Z}_k\}) \propto p(\boldsymbol{\theta}) p(\{\mathbf{Z}_k\} \,|\, \boldsymbol{\theta}) \tag{3}$$

where $p(\boldsymbol{\theta})$ denotes the prior PDF that reflects the plausibility of $\boldsymbol{\theta}$ in the absence of data. Assuming uniform prior information, the posterior PDF $p(\boldsymbol{\theta}|\{\mathbf{Z}_k\})$ is proportional to the 'likelihood function' $p(\{\mathbf{Z}_k\}|\boldsymbol{\theta})$. The 'most probable value' (MPV) of the modal parameters $\boldsymbol{\theta}$ can be determined by maximizing $p(\boldsymbol{\theta}|\{\mathbf{Z}_k\})$ and hence $p(\{\mathbf{Z}_k\}|\boldsymbol{\theta})$.

For large N and small Δt, the FFT at different frequencies can be shown to be asymptotically independent and follow a Gaussian distribution (Yuen and Katafygiotis 2003). The likelihood function $p(\{\mathbf{Z}_k\}|\boldsymbol{\theta})$ can be given by

$$p(\{\mathbf{Z}_k\} \,|\, \boldsymbol{\theta}) = \prod_k (2\pi)^{\ n} (\det \mathbf{C}_k)^{\ 1/2} \exp[\ \frac{1}{2} \mathbf{Z}_k^T \mathbf{C}_k^{\ 1} \mathbf{Z}_k] \tag{4}$$

where $\det(.)$ is the determinant

$$\mathbf{C}_k = \frac{1}{2} \begin{bmatrix} \boldsymbol{\Phi} & \\ & \boldsymbol{\Phi} \end{bmatrix} \begin{bmatrix} \mathrm{Re}\,\mathbf{H}_k & -\mathrm{Im}\,\mathbf{H}_k \\ \mathrm{Im}\,\mathbf{H}_k & \mathrm{Re}\,\mathbf{H}_k \end{bmatrix} \begin{bmatrix} \boldsymbol{\Phi}^T & \\ & \boldsymbol{\Phi}^T \end{bmatrix} + \frac{S_e}{2} \mathbf{I}_{2n} \tag{5}$$

denotes the covariance matrix of $\mathbf{Z}_k$, in which $\boldsymbol{\Phi} = [\boldsymbol{\varphi}_1, \boldsymbol{\varphi}_2, \ldots, \boldsymbol{\varphi}_m] \in R^{n \times m}$ is the mode shape matrix; m is the number of modes in a selected frequency band; S_e denotes the PSD of the prediction error; $\mathbf{I}_{2n} \in R^{2n}$ is the identity matrix; $\mathbf{H}_k \in R^{m \times m}$ denotes the transfer matrix and the (i, j) element of this matrix is given by

$$\mathbf{H}_k(i, j) = S_{ij}[(\beta_{ik}^2 - 1) + 2\mathbf{i}\zeta_i \beta_{ik}]^{-1}[(\beta_{jk}^2 - 1) - 2\mathbf{i}\zeta_j \beta_{jk}]^{-1} \tag{6}$$

where $\beta_{ik} = f_i/f_k$; f_k denotes the FFT frequency abscissa; f_i denotes the natural frequency of the ith mode; ζ_j denotes the damping ratio of the jth mode; S_{ij} denotes the cross spectral density between the ith and jth modal excitations. For analytical and computational purposes, it is convenient to work with the NLLF $L(\boldsymbol{\theta})$

$$L(\boldsymbol{\theta}) = \frac{1}{2} \sum_k [\ln \det \mathbf{C}_k(\boldsymbol{\theta}) + \mathbf{Z}_k{}^T \mathbf{C}_k(\boldsymbol{\theta})^{-1} \mathbf{Z}_k] \tag{7}$$

so that

$$p(\boldsymbol{\theta} \,|\, \{\mathbf{Z}_k\}) \propto \exp[-L(\boldsymbol{\theta})] \tag{8}$$

By this way, minimizing $L(\boldsymbol{\theta})$ is equivalent to maximizing $p(\boldsymbol{\theta}|\{\mathbf{Z}_k\})$.

The MPV of $\boldsymbol{\theta}$ can be determined by numerically minimizing the NLLF. However, the minimization process is ill-conditioned. On the other hand, the computational time grows drastically with the number of measured degrees of freedom. Therefore, in real applications, fast algorithms have been developed recently which allow the MPV to be obtained almost instantaneously in the case of well separated modes (Au 2011, Zhang and Au 2013) and closely-spaced modes (Au 2012a, b).

5. Analysis of monitoring data

5.1 Wenchuan Earthquake

5.1.1 Investigation in time and frequency domains

In this section, the responses in the time domain will be first investigated. Compared with other structural portions of the bridge, the towers would be more sensitive to the earthquake excitation due to two properties: firstly, the towers are slender, making significant vibration on the top of the tower; secondly, the traffic loading has less influence on the towers in comparison with the deck and cables.

Fig. 2 shows the time history of the seismic responses at the towers, where the first two subfigures correspond to the acceleration responses measured at the Tsing Yi tower, while the third one is the displacement response measured at the Ma Wan tower. The two acceleration responses at the Tsing Yi tower caused by the earthquake can be observed obviously, where a sudden increase in the response is observed at about 500 seconds after the earthquake's occurrence at the epicenter. The response measured by the displacement sensor installed at the Ma Wan tower also gradually increases, although it is not as obvious as the acceleration measured at the Tsing Yi tower. This is reasonable and consistent with the seismic wave propagation time between the epicenter and Hong Kong (1,440 km). The distance between the Ma Wan tower and the Tsing Yi tower is 1,377 m. The arriving time difference between the two towers should be less than 0.5 second. However, the sampling frequency is 2.56 Hz for the sensors installed on the towers. It is difficult to find the arriving time lag between the two towers.

The time-domain seismic responses at the deck and anchorage are also investigated. Fig. 3 shows the time history of the seismic responses acquired from some typical channels of sensors located at the deck and anchorage. It is not easy to judge the earthquake-induced responses at these locations. The ambient vibration at the deck and anchorage could be excited by different effects, e.g., the traffic loading due to highway and railway, wind loading, and ground tremor. When the magnitude of these loadings is similar to or larger than the excitation due to the earthquake, it is difficult to observe the response change in the time domain.

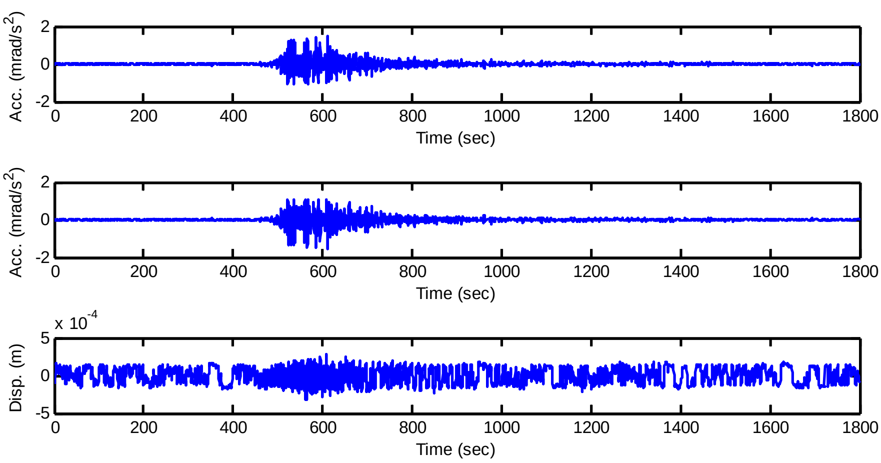

Fig. 2 Time history of seismic responses at bridge towers during Wenchuan Earthquake

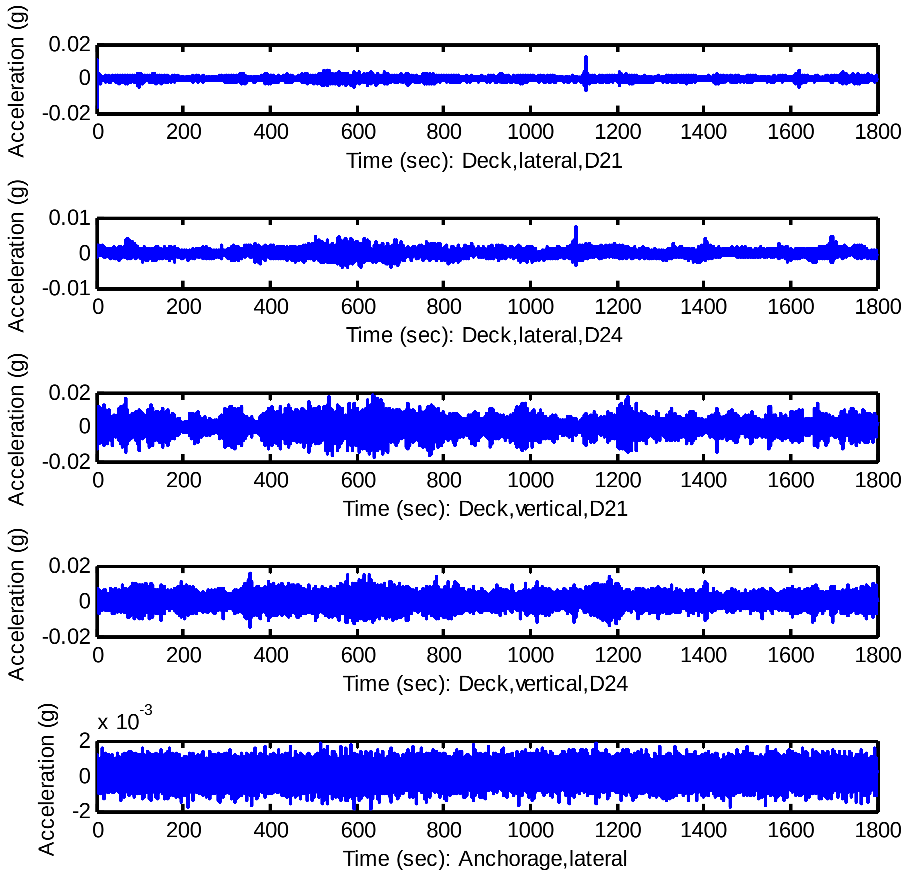

Fig. 3 Time history of accelerations measured at bridge deck and anchorage during Wenchuan Earthquake

The response data acquired from the sensors placed on the cables are expected for the investigation of time lag in this event. Two sensors instrumented at the main cables over the Ma Wan side span (Sensor C21) and the Tsing Yi side span (Sensor C26) respectively are selected, from which the response time histories are obtained as shown in Fig. 4 (the duration from 500s to 700s after the earthquake's occurrence at the epicenter, lateral direction). The first subfigure corresponds to the cable response over the Ma Wan side span, while the second one corresponds to that on the Tsing Yi side span. The distance between these two sensors are the biggest among all the installed sensors on the cables. Note that different from the data collected on the towers, the sampling frequency of the data acquired from the sensors on the main cables is 51.2 Hz. This means that even in 0.5 second, there will be about 25 sampling points collected, which make it possible to perform the time lag investigation. The response in the vertical direction (not shown here) due to the earthquake is not obvious while the one in the lateral direction can be observed clearly as shown in the figure. Time lag of the responses at the two side spans is observed. It seems that the earthquake arrived at the Tsing Yi side span a little earlier. This is consistent with the fact that the Tsing Yi Island is a little near to the epicenter. From the magnitude of the acceleration, it is seen that the response of the main cable over the Ma Wan side span is much higher than that

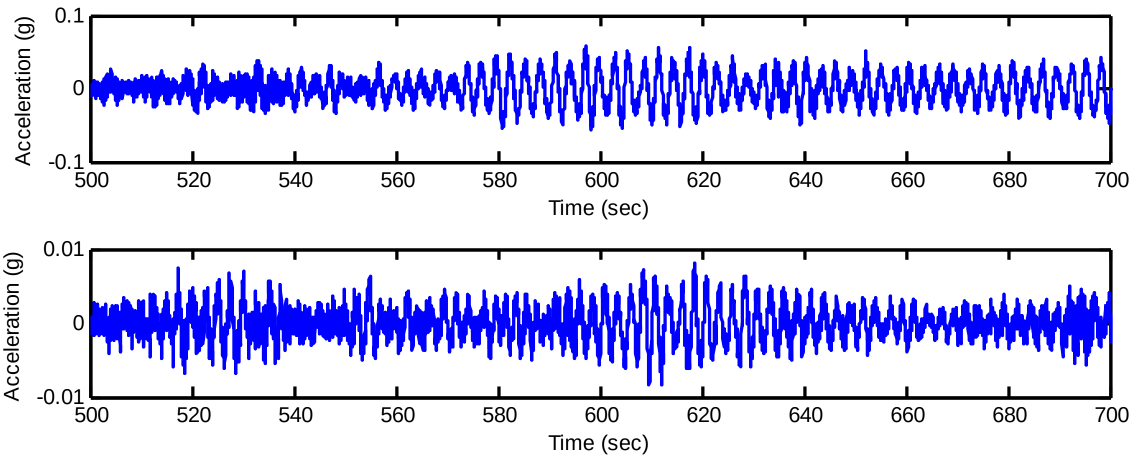

Fig. 4 Time history of seismic responses at main cables during Wenchuan Earthquake

over the Tsing Yi side span. This is reasonable because on the Ma Wan side span the main cables are connected with the deck by hangers, while on the Tsing Yi side span the deck is supported by three piers instead of being connected to the main cables by hangers; the seismic response of the deck at the Tsing Yi side span couldn't be directly transmitted to the main cables over this side span because of the absence of hangers.

Next, we take a close look into Fig. 5 by zooming in Fig. 4 with only 50-sec data, i.e., from 600s to 650s after the earthquake's occurrence at the epicenter. It is seen that an evident wave phase exists between the two responses. The response in the upper figure covers about 17 cycles of vibration, while the response in the lower figure involves about 20 cycles of vibration. This indicates that the dominant frequencies excited by the seismic loading are different at the two sides, making it difficult to investigate the exact wave phase between the two side spans of the bridge. On the other hand, it is shown that the different structural portions of the bridge under seismic loading could have different behaviors. This may be also because the frequencies of the earthquake wave are different when propagating to different locations. From the data in the time domain, it is difficult to investigate the influence of the seismic excitation, especially on the deck and anchorage. To better understand the influence, the response data are further analyzed in the frequency domain. As shown in Fig. 2, only about 300-sec responses (around 500s to 800s) at the tower are influenced by the earthquake excitation. In recognizing this fact, we select a 300-sec data segment respectively from Data 1, Data 2 (the data segment from Data 2 is exactly covering the duration of seismic response), and Data 3 as the data sets before, during and after the earthquake respectively, to perform spectral analysis and study the structural behavior before, during and after the earthquake.

Fig. 6 shows the root power spectral density (PSD) spectra of the vertical accelerations at the bridge deck before, during and after the earthquake. It is interesting to see that the frequency-domain response components at the first few modes in Fig. 6(b) are obviously larger than those in Fig. 6(a), (c). This means that the lower modes are influenced by the earthquake obviously, which may be attributed to the attenuation of higher-frequency ingredients of the seismic wave in long-

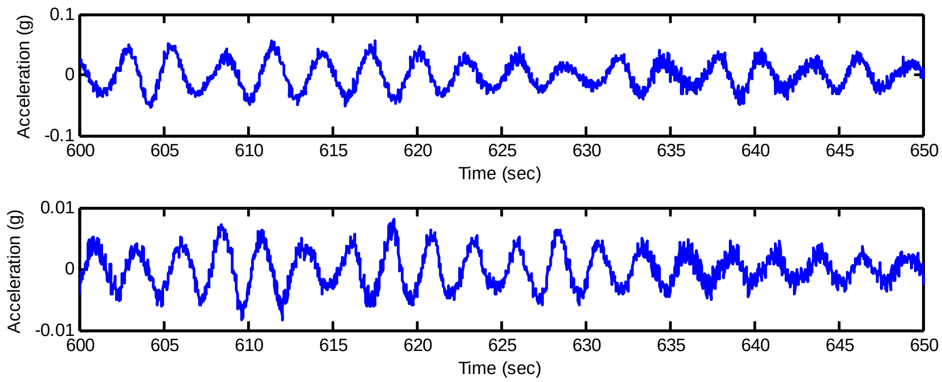

Fig. 5 Close-up view of seismic responses at main cables during Wenchuan Earthquake

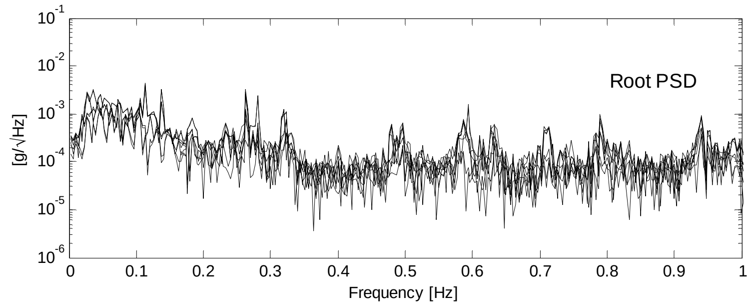

(a) Before the earthquake

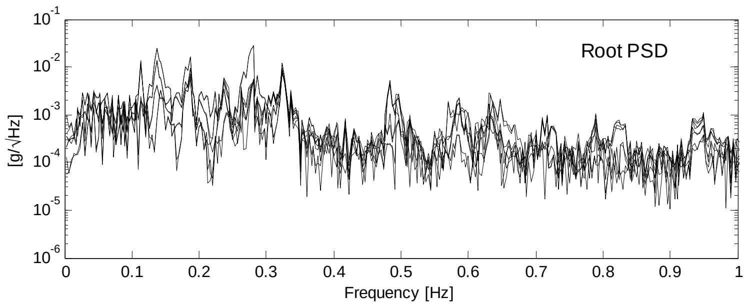

(b) During the earthquake

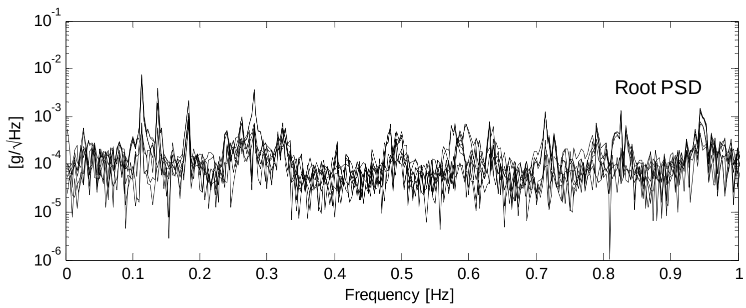

(c) After the earthquake

Fig. 6 PSD spectra of vertical accelerations at bridge deck before, during and after Wenchuan Earthquake

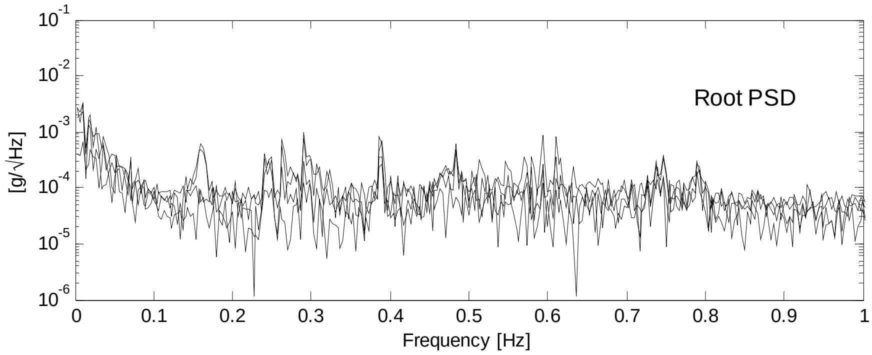

(a) Before the earthquake

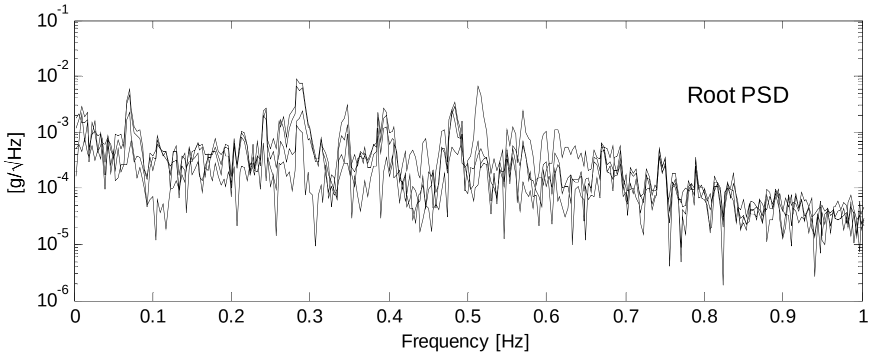

(b) During the earthquake

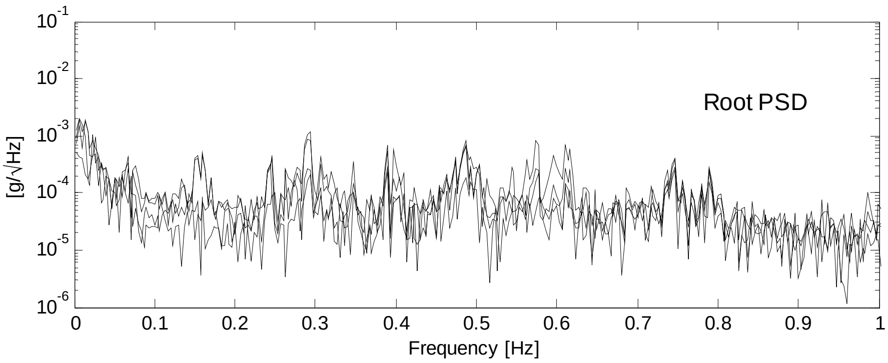

(c) After the earthquake

Fig. 7 PSD spectra of lateral accelerations at bridge deck before, during and after Wenchuan Earthquake

distance propagation from the epicenter to Hong Kong. After long-distance propagation, only lower-frequency components remain in the seismic wave and produce obvious excitation to the bridge.

In the lateral direction, similar observation is obtained as in the vertical direction. Fig. 7 shows the PSD spectra of the measured deck responses in the lateral direction. It is seen that in Fig. 7(a), (c), the modal response at the frequency around 0.068 Hz is not obvious, especially in Fig. 7(a), where the response peak at this frequency is almost drowned by the noise. Another one is the

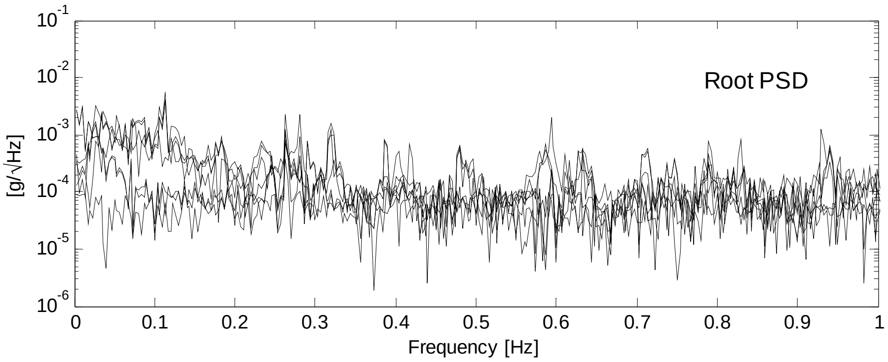

(a) Before the earthquake

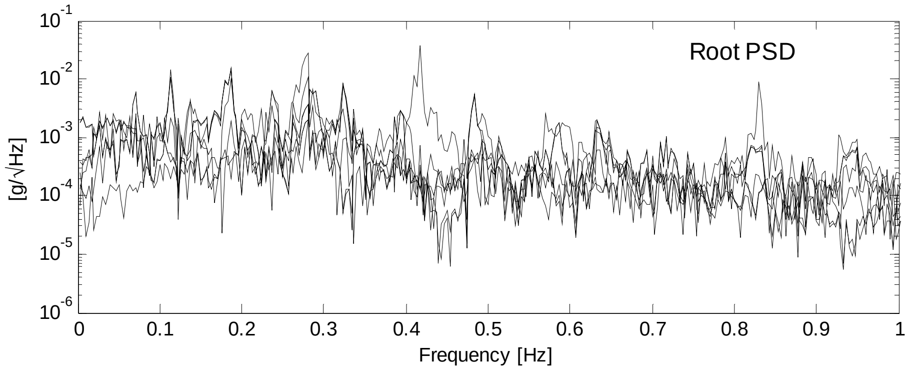

(b) During the earthquake

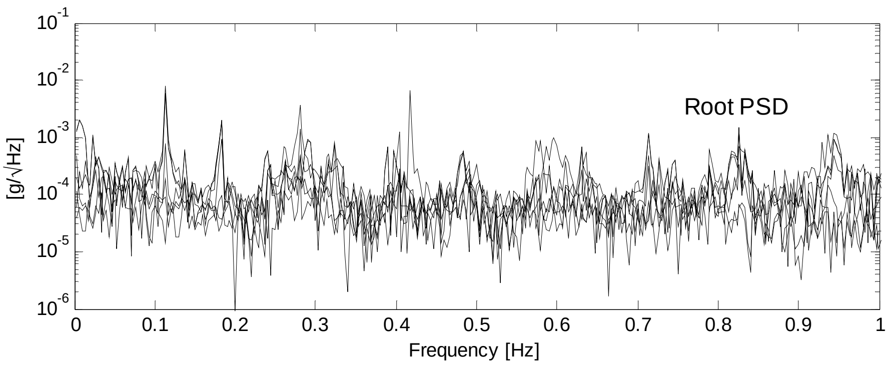

(c) After the earthquake

Fig. 8 PSD spectra of vertical accelerations at main cables before, during and after Wenchuan Earthquake

modal response at the frequency around 0.52 Hz. The modal responses at these two frequencies in Fig. 7(b) are much higher than those shown in Fig. 7(a), (c), indicating a significant influence of the long-distance earthquake on the lower-frequency response components.

A similar observation is obtained in the main cables. As shown in Fig. 8, the long-distance earthquake generates the vertical response of the main cables at the frequencies around 0.2 Hz, 0.45 Hz and 0.85 Hz. The lateral response of the main cables is mainly excited at the frequencies around 0.07Hz and 0.35 Hz, as shown in Fig. 9. The lateral response amplitudes at these two frequencies during the earthquake are much higher than those before and after the earthquake.

Fig. 10 shows the PSD spectra of the accelerations measured at the anchorage before, during

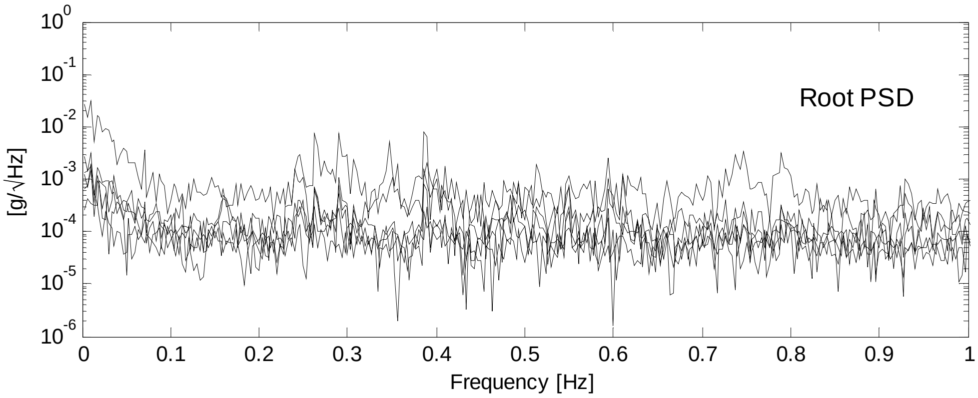

(a) Before the earthquake

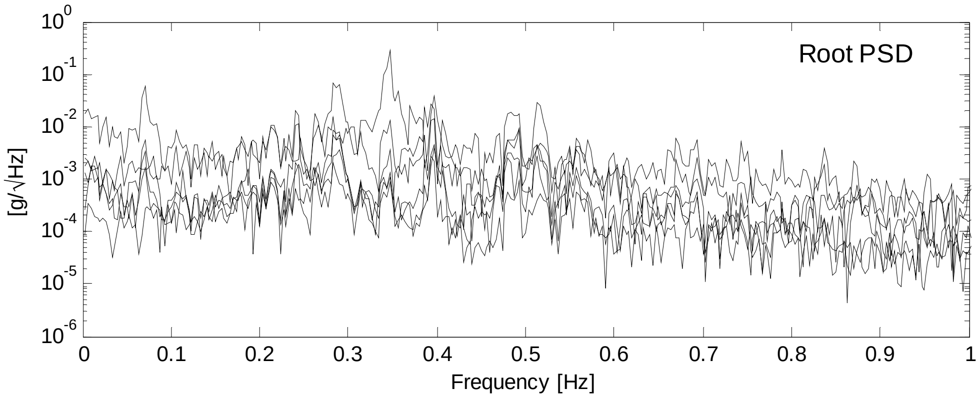

(b) During the earthquake

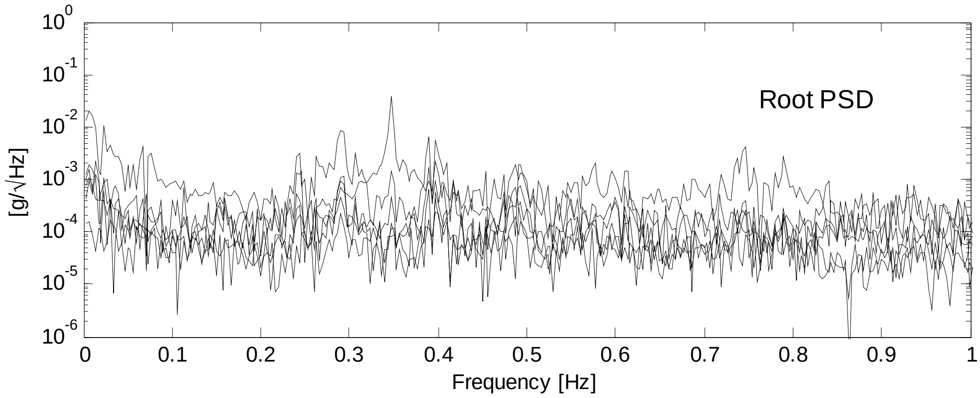

(c) After the earthquake

Fig. 9 PSD spectra of lateral accelerations at main cables before, during and after Wenchuan Earthquake

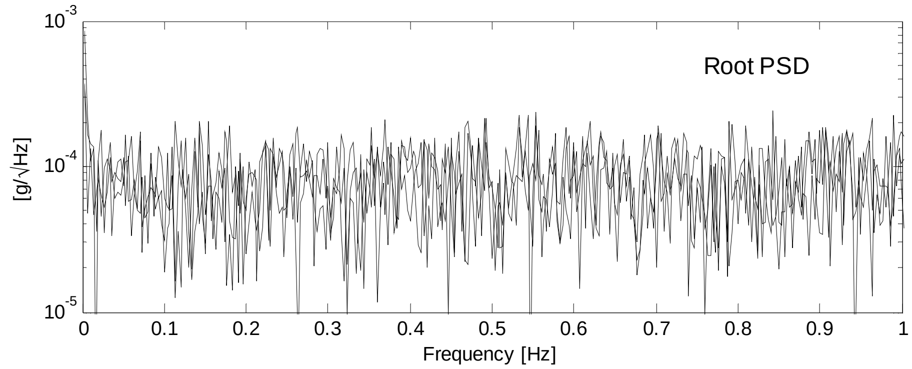

(a) Before the earthquake

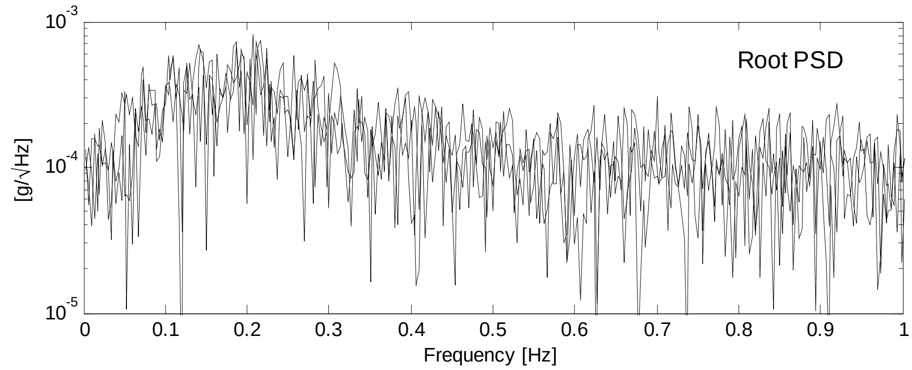

(b) During the earthquake

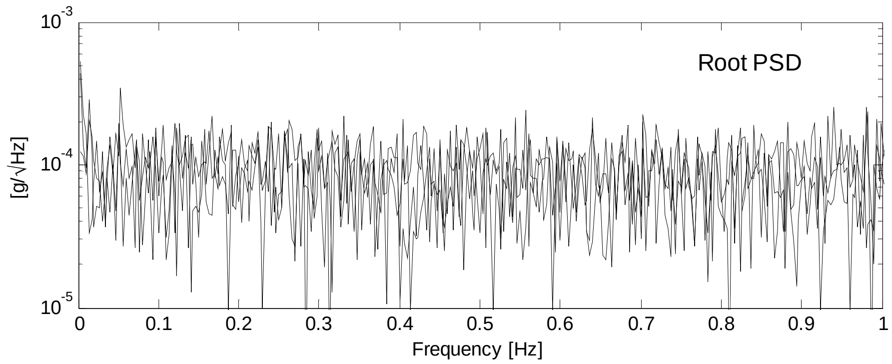

(c) After the earthquake

Fig. 10 PSD spectra of accelerations at anchorage before, during and after Wenchuan Earthquake

and after the earthquake. It is seen that the spectral components at 0-0.4 Hz in Fig. 10(b) are much higher than those in other two subfigures. As mentioned before, however, no big difference is observed among the three sets of data in the time domain. It is believed that this is also due to the seismic loading with low-frequency components.

5.1.2 Operational modal analysis

The fast Bayesian FFT method is applied to the ambient vibration responses recorded from the deck. A merit of the Bayesian method is that it can identify the power spectral density (PSD) of the modal force, which is an important quantity to evaluate the excitation. Three modal parameters, i.e., modal frequency, damping ratio, and the PSD of modal force, will be obtained. To compare the modal parameters before and after the earthquake, the fast Bayesian FFT method is applied to the two sets of data (Data 1 and Data 3) separately.

The present study focuses on the first twelve modes of the deck, i.e., the first six lateral modes (L1 to L6), the first four vertical modes (V1 to V4), the first torsional mode (T1), and the first vertical mode of the Ma Wan side span (MWV1). When applying the fast Bayesian FFT method, frequency bands are selected whose FFT data shall be used for identifying the modes they cover. The selected frequency bands and the initial guess of the frequencies for the twelve modes are shown in Table 1.

Fig. 11 and Fig. 12 show the mode shapes identified before the earthquake in the vertical and lateral directions, respectively. Since the accelerometers located on the deck are limited, the finite element model (FEM) has been used to help identify the properties of the identified modes by comparing the identified modal vectors and the mode shapes calculated by the FEM. These results are consistent with the FEM well. Table 2 shows the modal assurance criterion (MAC) between the modal vectors identified before and after the earthquake for all the identified modes in the vertical and lateral directions. It is seen that the MAC values are all close to 1. This indicates that there is no much change of the mode shapes before and after the earthquake.

Table 3 and Table 4 show the modal parameters of the vertical modes identified using the data before and after the earthquake, respectively. It is seen that the natural frequencies of these six modes are all less than 0.3 Hz, while the damping ratios are all less than 1%. This is consistent with the properties of long-span suspension bridges. The natural frequencies of Modes V3, V4 and T1 have a slight increase after the earthquake while the damping ratios of Modes V1, V2 V3, V4 and MWV1 decrease. Since the change of natural frequency is small, it is difficult to judge whether this is attributed to the earthquake effect. The fourth column in the tables shows the identified PSD of modal force. It is seen that in Table 3 and Table 4 for the modes in the main span, there is a decreasing trend, i.e., the contribution of the modes in the bridge decreases with the increase

Table 1 Initial guess and frequency band used in modal identification

Mode		V1	V2	V3	V4	T1	MWV1	L1	L2	L3	L4	L5	L6
Initial guess	f_0 (Hz)	0.114	0.136	0.183	0.238	0.264	0.280	0.068	0.160	0.241	0.246	0.265	0.289
Band	f_1 (Hz)	0.107	0.130	0.177	0.227	0.256	0.271	0.063	0.144	0.237	0.243	0.258	0.276
	f_2 (Hz)	0.120	0.145	0.191	0.248	0.269	0.295	0.075	0.177	0.243	0.251	0.272	0.302

Table 2 MAC values before and after Wenchuan Earthquake

Vertical mode	V1	V2	V3	V4	T1	MWV1
MAC	1.000	1.000	1.000	0.999	0.999	1.000
Lateral mode	L1	L2	L3	L4	L5	L6
MAC	0.999	0.998	0.979	0.972	0.993	1.000

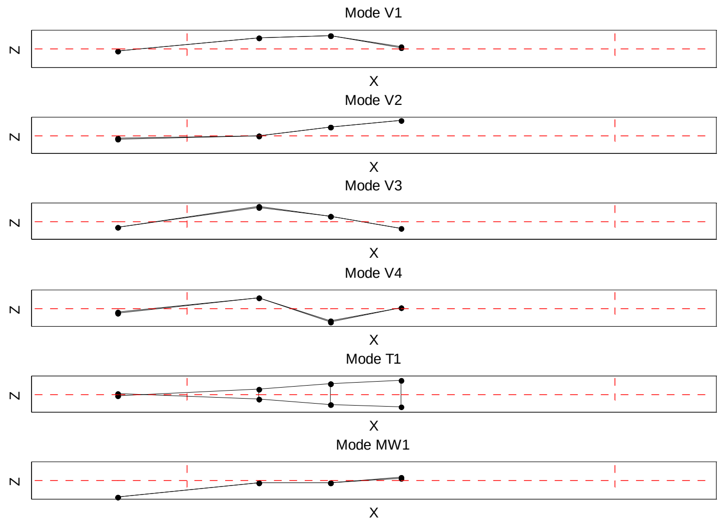

Fig. 11 Mode shape in vertical direction, before Wenchuan Earthquake

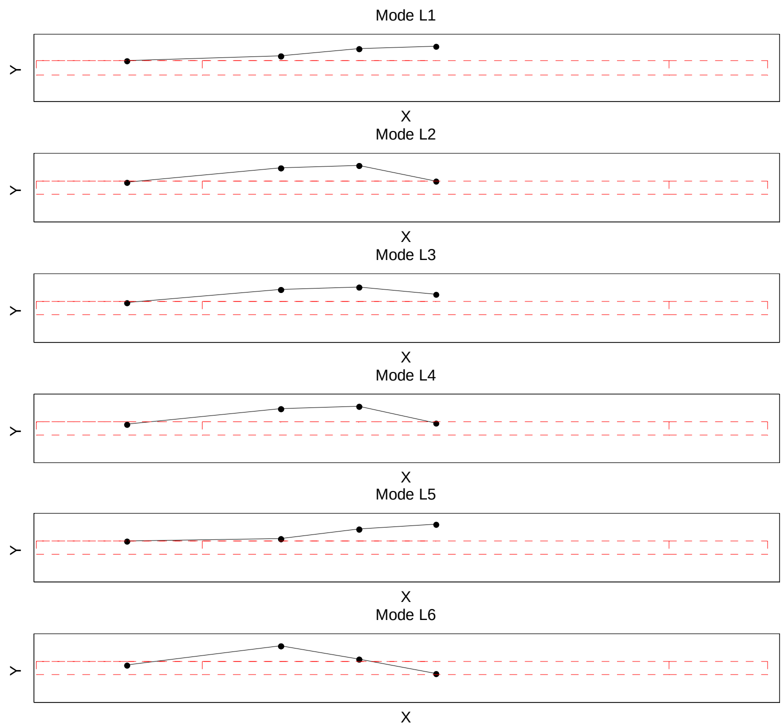

Fig. 12 Mode shape in lateral direction, before Wenchuan Earthquake

of the mode order under nominal conditions. Table 5 and Table 6 show the identified modal parameters of six lateral modes of the deck. The natural frequencies of these modes are all also less than 0.3 Hz with the first mode less than 0.1 Hz. The damping ratios in the first two modes

Table 3 Identified modal parameters of vertical modes of bridge deck before Wenchuan Earthquake

Mode	f (Hz)	COV (%)	Damping ratio (%)	COV (%)	S ($10^{-9}g^2$/Hz)	COV (%)
V1	0.114	0.21	0.52	45.7	49.8	24.4
V2	0.136	0.20	0.53	41.3	13.9	23.3
V3	0.182	0.19	0.57	37.1	1.3	25.0
V4	0.237	0.18	0.67	31.1	0.6	22.7
T1	0.264	0.06	0.10	69.7	0.4	25.9
MWV1	0.279	0.12	0.39	33.1	2.3	17.9

Table 4 Identified modal parameters of vertical modes of bridge deck after Wenchuan Earthquake

Mode	f (Hz)	COV (%)	Damping ratio (%)	COV (%)	S ($10^{-9}g^2/Hz$)	COV (%)
V1	0.114	0.18	0.36	49.2	22.5	24.2
V2	0.136	0.19	0.47	43.3	18.3	22.7
V3	0.183	0.14	0.36	42.7	0.8	22.9
V4	0.238	0.15	0.48	34.2	0.5	21.6
T1	0.265	0.13	0.36	40.5	0.6	30.4
MWV1	0.279	0.09	0.25	39.4	3.2	17.2

Table 5 Identified modal parameters of lateral modes of bridge deck before Wenchuan Earthquake

Mode	f (Hz)	COV (%)	Damping ratio (%)	COV (%)	S ($10^{-9}g^2$/Hz)	COV (%)
L1	0.068	0.51	1.22	47.5	0.46	39.8
L2	0.159	0.33	1.55	24.6	1.20	17.5
L3	0.242	0.16	0.38	52.2	0.04	52.3
L4	0.246	0.15	0.38	46.0	0.06	40.2
L5	0.265	0.08	0.12	59.7	0.01	37.1
L6	0.290	0.13	0.46	31.1	0.53	18.7

Table 6 Identified modal parameters of lateral modes of bridge deck after Wenchuan Earthquake

Mode	f (Hz)	COV (%)	Damping ratio (%)	COV (%)	S ($10^{-9}g^2$/Hz)	COV (%)
L1	0.068	0.46	1.14	43.6	1.18	30.8
L2	0.160	0.25	0.98	27.8	0.66	15.2
L3	0.242	0.18	0.43	52.5	0.02	55.8
L4	0.246	0.11	0.22	53.3	0.02	39.4
L5	0.266	0.17	0.55	37.4	0.04	33.0
L6	0.290	0.16	0.67	28.0	0.40	20.2

are relatively large (>1%). The damping ratio decreases obviously in Mode L2 while there is a slight change in other modes. It is interesting to see that before the earthquake, the PSD of modal force for Mode L1 is much less than that for Mode L2, but after the earthquake, its value increases in Mode L1 while decrease in Mode L2 obviously. This indicates that Mode L1 may be influenced

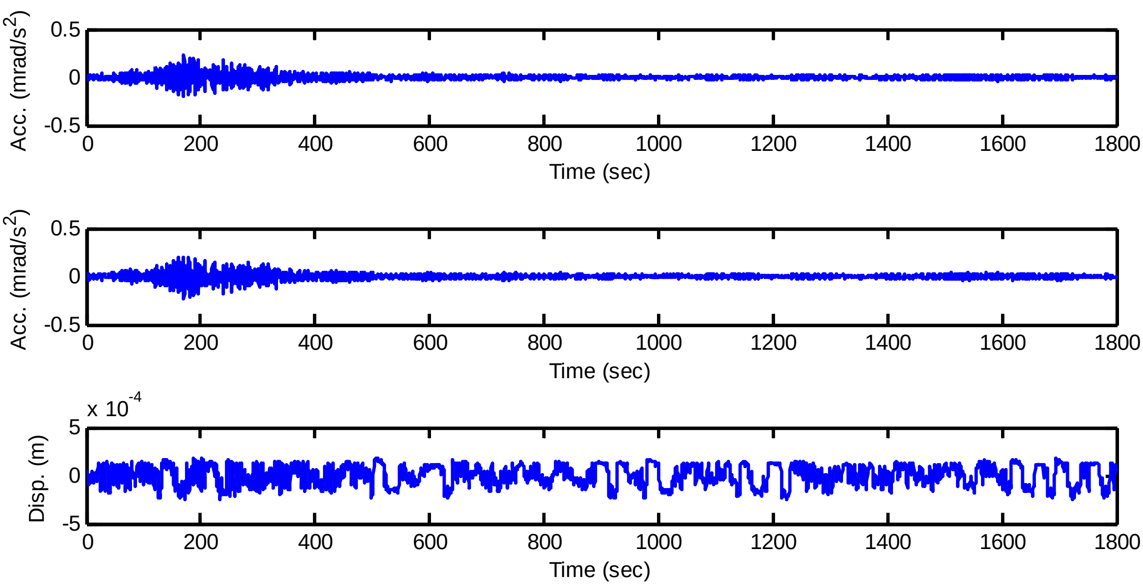

Fig. 13 Time history of seismic responses at bridge towers during Taiwan Earthquake

Table 7 Identified modal parameters of vertical modes of bridge deck before Taiwan Earthquake

Mode	f (Hz)	COV (%)	Damping ratio (%)	COV (%)	S (10^{-9}g^2/Hz)	COV (%)
V1	0.114	0.18	0.34	50.5	118.7	22.8
V2	0.137	0.14	0.21	50.9	13.5	21.6
V3	0.183	0.19	0.57	37.0	1.2	25.2
V4	0.239	0.20	0.77	32.7	0.4	27.9
T1	0.265	0.13	0.34	40.0	0.4	28.0
MWV1	0.281	0.10	0.27	37.8	1.4	17.2

Table 8 Identified modal parameters of vertical modes of bridge deck after Taiwan Earthquake

Mode	f (Hz)	COV (%)	Damping ratio (%)	COV (%)	S (10^{-9}g^2/Hz)	COV (%)
V1	0.114	0.21	0.49	46.1	68.6	23.8
V2	0.137	0.12	0.20	62.8	16.9	21.0
V3	0.183	0.14	0.33	43.5	1.0	22.3
V4	0.240	0.19	0.73	31.5	0.4	25.1
T1	0.266	0.09	0.19	47.0	0.2	25.7
MWV1	0.281	0.10	0.28	37.2	1.4	17.2

significantly by the earthquake excitation, which is consistent with the result in PSD spectra.

Next, we investigate the influence on the posterior uncertainty of the identified modal parameters due to the earthquake. In the above tables, in addition to the MPVs of the identified modal parameters, the corresponding coefficients of variation (COV=standard derivation/MPV)

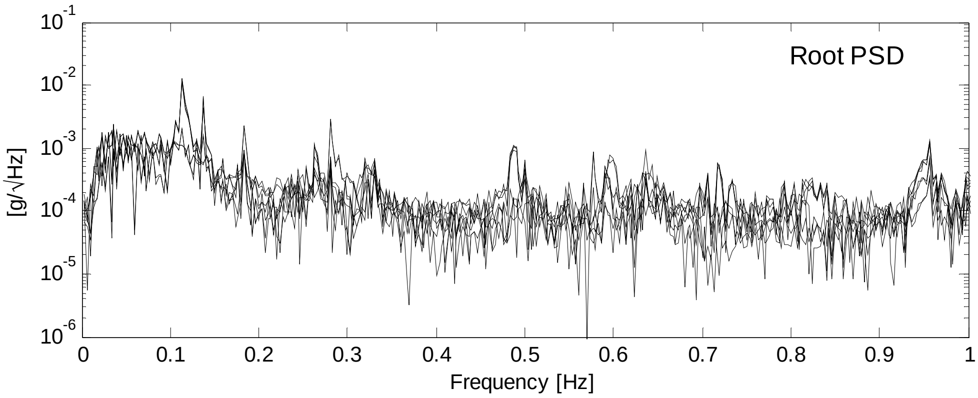

(a) Before the earthquake

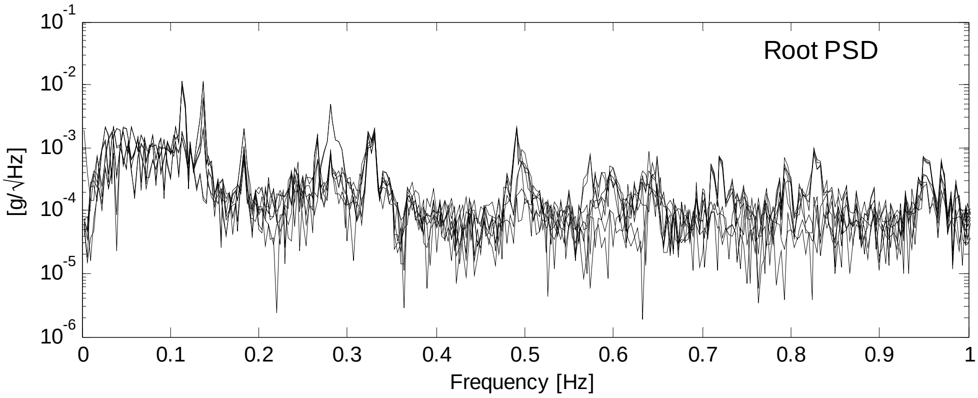

(b) During the earthquake

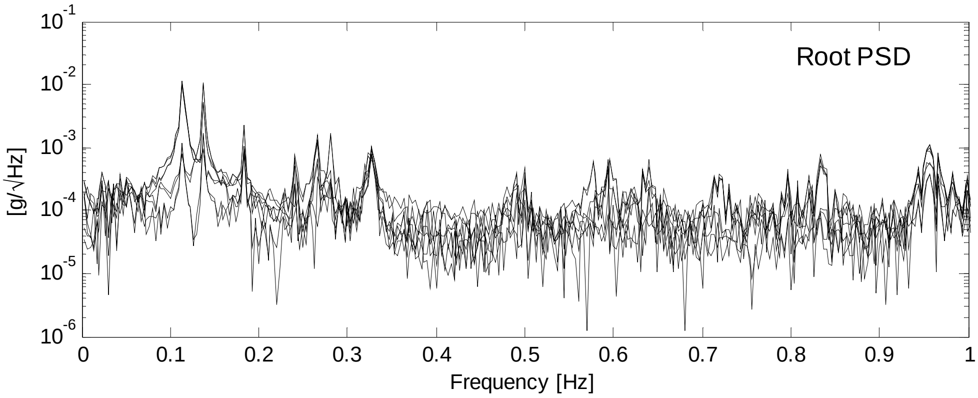

(c) After the earthquake

Fig. 14 PSD spectra of vertical accelerations at bridge deck before, during and after Taiwan Earthquake

are also presented. It is seen that the COVs of natural frequencies are very small in all the cases, in the order of less than 1%. While the damping ratios have a relatively large posterior uncertainty, their COVs are in the order of several tens percent. This is consistent with the fact that the

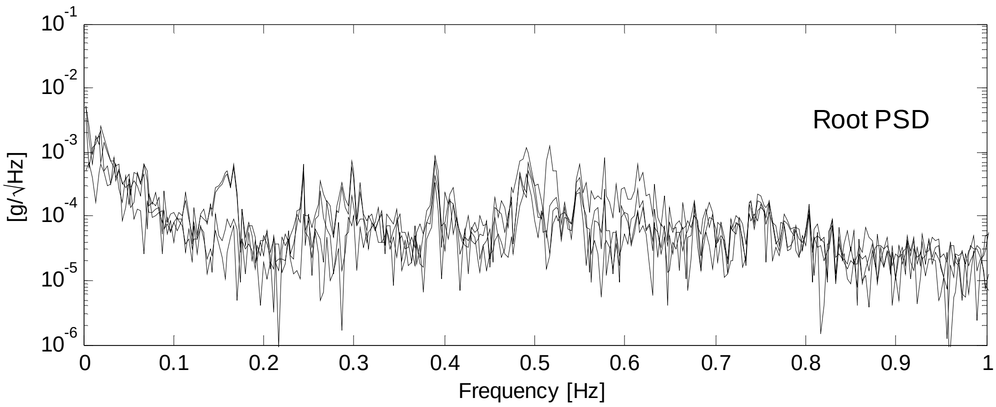

(a) Before the earthquake

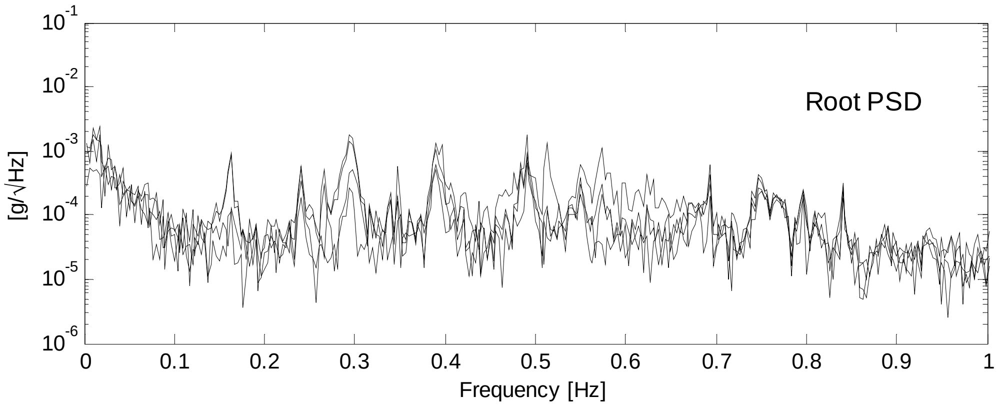

(b) During the earthquake

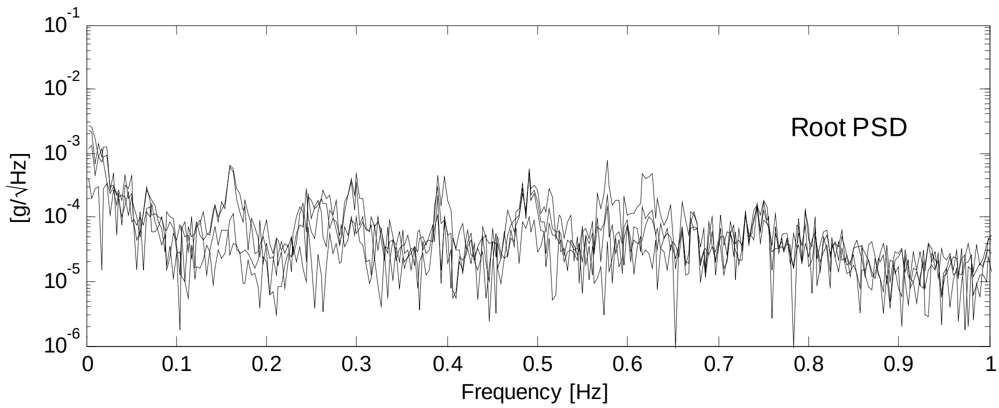

(c) After the earthquake

Fig. 15 PSD spectra of lateral accelerations at bridge deck before, during and after Taiwan Earthquake

damping ratio usually has a large variability. In the vertical direction, except Mode T1, the COVs of natural frequencies in other modes decrease after the earthquake while the COVs of damping ratio increase. This is not observed in the lateral modes.

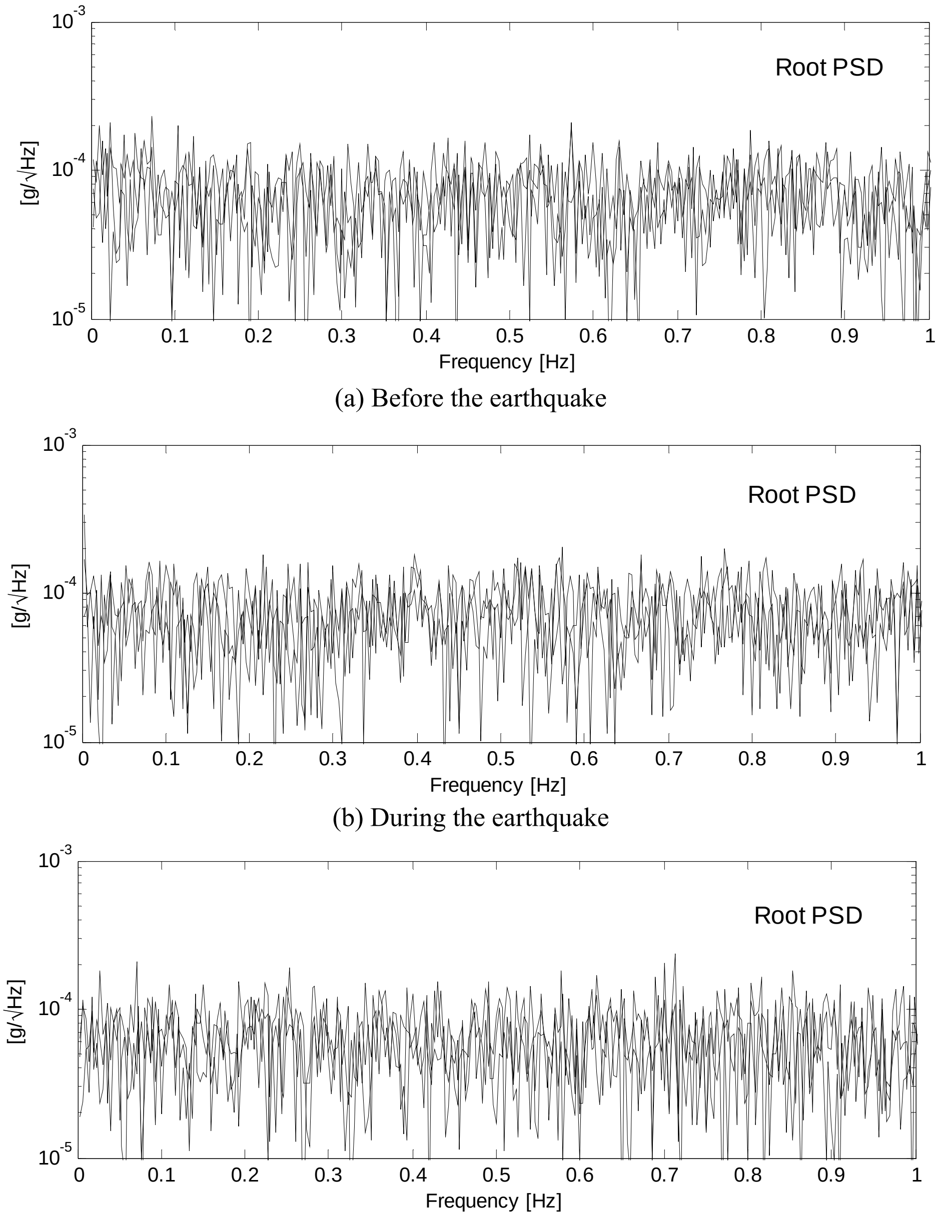

(a) Before the earthquake

(b) During the earthquake

(c) After the earthquake

Fig. 16 PSD spectra of accelerations at anchorage before, during and after Taiwan Earthquake

5.2 Taiwan Earthquake

As mentioned before, this event can be taken as a middle-distance earthquake according to the distance between the epicenter and Hong Kong. Fig. 13 shows the time history of the seismic responses at the towers with the start time at the moment of the earthquake's occurrence. Similar to the response during the Wenchuan Earthquake, the structural response caused by the Taiwan

Table 9 Identified modal parameters of lateral modes of bridge deck before Taiwan Earthquake

Mode	f (Hz)	COV (%)	Damping ratio (%)	COV (%)	S (10^{-9}g^2/Hz)	COV (%)
L1	0.068	0.29	0.52	62.9	0.26	34.7
L2	0.161	0.29	1.25	25.7	0.73	16.2
L3	0.242	0.15	0.29	52.3	0.02	47.5
L4	0.245	0.16	0.36	48.2	0.02	43.9
L5	0.266	0.15	0.42	41.9	0.02	36.1
L6	0.293	0.21	0.97	25.8	0.35	22.1

Table 10 Identified modal parameters of lateral modes of bridge deck after Taiwan Earthquake

Mode	f (Hz)	COV (%)	Damping ratio (%)	COV (%)	S (10^{-9}g^2/Hz)	COV (%)
L1	0.068	0.83	1.61	50.7	0.19	53.3
L2	0.161	0.28	1.15	26.8	0.57	17.1
L3	0.242	0.10	0.16	57.7	0.01	44.0
L4	0.246	0.12	0.21	58.5	0.02	47.9
L5	0.266	0.12	0.33	42.4	0.02	31.5
L6	0.291	0.23	1.07	26.0	0.38	23.6

Earthquake began to have an obvious increase at about 100 seconds after the earthquake's occurrence at the epicenter. This is consistent with the distance between the epicenter and Hong Kong (about 660 km). This sudden change has continued for about 300 seconds. Although the epicenter is much nearer than that of the Wenchuan Earthquake, the response caused by the Taiwan Earthquake is much lower than that due to the Wenchuan Earthquake. This is because the magnitude in the latter earthquake is 8.0, which is much higher than that in this event. Akin to the response during the Wenchuan Earthquake, there is also no obvious change in the displacement response due to this event, as illustrated in the third subfigure of Fig. 13. Different from the responses at the towers, it is difficult to find a change of the response time histories at the deck, main cables and anchorage caused by the earthquake.

For the responses measured at the towers (Fig. 13), only about 300 sec responses (around 100s to 400s) are influenced by the earthquake excitation. Similar to the case of the Wenchuan Earthquake, we select 300 sec data before the earthquake, 300 sec data which exactly cover the earthquake response, and 300 sec data after the earthquake to perform spectral analysis and study the structural behavior before, during and after earthquake. Fig. 14 shows the root PSD spectra of the vertical responses at the bridge deck for the three sets of data acquired before, during and after the earthquake. Different from the case in the Wenchuan Earthquake, there is no obvious change among the three spectra. This phenomenon is also observed in the three PSD spectra of the deck responses in the lateral direction, as shown in Fig. 15. To further understand the influence of the earthquake, the modal parameters are identified using the two sets of data before and after the earthquake and the identification results are shown in Table 7 and Table 8 for the vertical modes and in Table 9 and Table 10 for the lateral modes. Different from the case in the Wenchuan Earthquake, the PSD of modal force for Mode L1 decreases slightly in this event. There is no obvious trend for other modal parameters. Fig. 16 shows the PSD spectra of the accelerations measured at the anchorage. From this figure, it is interesting to observe that the higher spectrum appearing during the Wenchuan Earthquake cannot be found during this earthquake event. This evidences that the frequency components of seismic excitation are different in the middle-distance earthquake and in the long-distance earthquake. Furthermore, by evaluating the MAC values (not shown here) of the modal vectors identified before and after the earthquake, similar to the case in the Wenchuan Earthquake, the MAC values are quite close to 1 and there is no much change for the mode shapes.

5.3 Heyuan Earthquake

Fig. 17 shows the time history of the seismic responses at the towers with the start time at the moment of the earthquake's occurrence. It is seen that there is an increase in the response amplitude at about 40 seconds after the earthquake's occurrence at the epicenter. However, due to the change is not obvious, it is difficult to judge whether it is exactly caused by the earthquake. The magnitude of the earthquake is the smallest among the three ones addressed in this study, although it is the one nearest to Hong Kong. Again, the most sensitive structural portion to the seismic loading is the towers. The response due to the earthquake cannot be obviously observed in other structural portions such as the deck, main cables and anchorage in the time domain (not shown here) due to the relatively large ambient excitation. Consistent to the observation in the time domain, there is no significant change in PSD spectra (not shown here) before, during and after the earthquake. Table 11 to Table 12 and Table 13 to Table 14 provide the identified modal parameters of the vertical and lateral modes of the deck, respectively. Consistent with the findings in the Taiwan Earthquake, there is slight change for the PSD of modal force for Mode L1 after the earthquake. This indicates that the change of this quantity in the Wenchuan Earthquake is not accidental and is believed to be influenced by the long-distance earthquake. For the mode shapes (not shown here), there is no any significant change subjected to the earthquake. In summary, there is no obvious effect of this earthquake on the bridge.

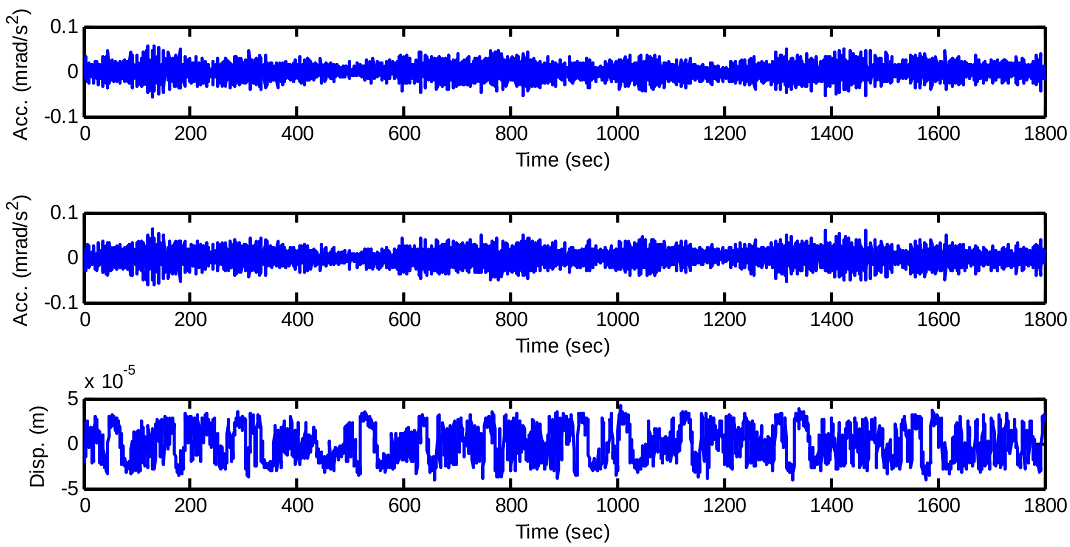

Fig. 17 Time history of seismic responses at bridge towers during Heyuan Earthquake

The PSD spectra of the accelerations measured at the anchorage before, during and after the earthquake are also studied. Similar to the Taiwan Earthquake case, no obvious change is observed during this earthquake event. This may explain why the responses at the superstructure caused by the earthquake are not obvious.

From this event, it is seen that when the magnitude of the earthquake is not large, even if the

Table 11 Identified modal parameters of vertical modes of bridge deck before Heyuan Earthquake

Mode	f (Hz)	COV (%)	Damping ratio (%)	COV (%)	S ($10^{-9}g^2$/Hz)	COV (%)
V1	0.115	0.32	1.01	37.7	80.4	29.0
V2	0.136	0.26	0.83	36.2	41.3	25.5
V3	0.182	0.20	0.63	36.4	1.6	26.4
V4	0.237	0.23	0.94	30.4	0.6	27.0
T1	0.265	0.11	0.27	44.2	0.6	29.8
MWV1	0.279	0.09	0.21	42.4	2.2	18.0

Table 12 Identified modal parameters of vertical modes of bridge deck after Heyuan Earthquake

Mode	f (Hz)	COV (%)	Damping ratio (%)	COV (%)	S ($10^{-9}g^2$/Hz)	COV (%)
V1	0.114	0.32	0.99	37.6	97.2	28.0
V2	0.136	0.20	0.53	41.5	30.4	23.9
V3	0.182	0.19	0.56	37.7	1.3	26.1
V4	0.238	0.16	0.52	33.8	0.6	22.9
T1	0.265	0.18	0.57	38.5	0.7	36.2
MWV1	0.279	0.11	0.33	35.6	2.2	18.3

Table 13 Identified modal parameters of lateral modes of bridge deck before Heyuan Earthquake

Mode	f (Hz)	COV (%)	Damping ratio (%)	COV (%)	S ($10^{-9}g^2$/Hz)	COV (%)
L1	0.067	0.52	1.29	46.7	0.89	39.2
L2	0.161	0.27	1.09	26.8	0.88	15.8
L3	0.242	0.09	0.14	66.4	0.02	43.4
L4	0.246	0.06	0.11	88.6	0.03	38.7
L5	0.265	0.10	0.21	52.6	0.01	38.4
L6	0.292	0.12	0.36	35.7	0.29	23.3

Table 14 Identified modal parameters of lateral modes of bridge deck after Heyuan Earthquake

Mode	f (Hz)	COV (%)	Damping ratio (%)	COV (%)	S ($10^{-9}g^2$/Hz)	COV (%)
L1	0.068	0.30	0.57	54.9	0.85	27.9
L2	0.161	0.22	0.81	29.7	0.90	15.2
L3	0.242	0.05	0.06	193.3	0.01	48.5
L4	0.246	0.13	0.31	48.5	0.04	39.4
L5	0.266	0.14	0.34	46.2	0.01	39.9
L6	0.290	0.11	0.31	39.3	0.32	26.1

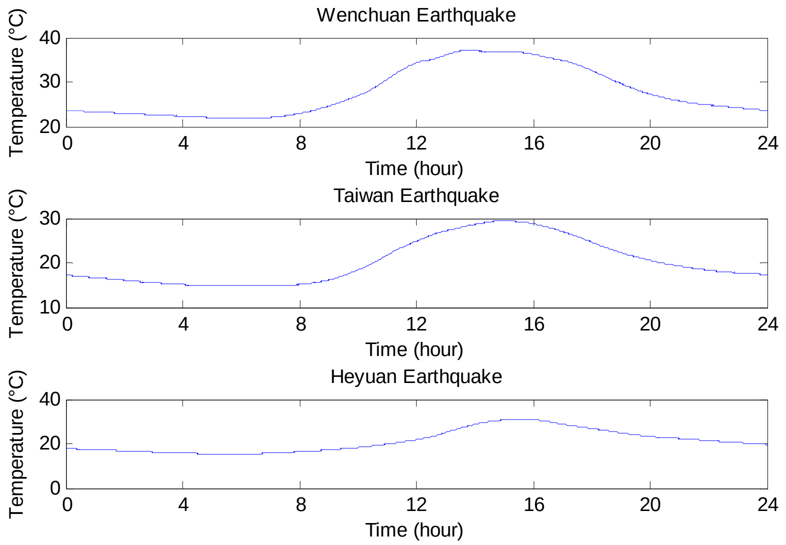

Fig. 18 Temperature variation in three earthquake events (from 0:00 to 24:00)

epicenter is quite near to the subjected structure, its effect on TMB is very limited. This is reasonable because the ambient excitations, e.g., highway and railway traffic, wind loading, may be still dominant for TMB in low-magnitude earthquake case.

5.4 Temperature effect

In the recent studies, it is found that temperature variation may have significant effect on the modal parameters of subjected structures (Ni *et al.* 2005, Xia *et al.* 2006, Yuen and Kuok 2010, Casciati *et al.* 2014). In the SHM system of the Tsing Ma Bridge, temperature sensors are also instrumented on the deck and cable of this structure, making it possible to investigate this effect. Since deck is mainly focused on in the modal identification of this study, a representative temperature sensor on the deck close to the Ma Wan tower is chosen. Fig. 18 shows the temperature variation in the days when the three earthquakes happened. The temperature varies obviously from mid-night to the afternoon in each event. Recall that the three earthquakes happened in 14:28 (Wenchuan), 20:28 (Taiwan) and 11:34 (Heyuan) respectively and only one hour of data (30 min each for the investigation before and after earthquake) is utilized for modal identification. It is seen from Fig. 18 that there is no much temperature variation for the three events in the duration related to our study. Therefore, the temperature effect can be ignored in this study.

6. Conclusions

This paper presents the work on the operational modal analysis of the Tsing Ma Bridge (TMB) situated in Hong Kong during three earthquakes, i.e., long-, middle- and short-distance earthquakes with the use of the Fast Bayesian FFT method. In these three events, it is seen that the towers are the most sensitive structural portion of the bridge to the earthquakes, and the seismic responses caused by the earthquakes are not obvious for other structural portions such as the deck, main cables and anchorage. On the responses at the towers, the influence of the earthquakes on the acceleration response is more significant than the displacement response. Although the distance between Wenchuan city and Hong Kong is the farthest among the three earthquakes, since the magnitude of this event is the largest, its influence on the bridge is the most evident. By comparing the acceleration responses of the main cables over the Ma Wan side span and over the Tsing Yi side span, the time lag of the seismic response can be observed. The dominant vibration behavior of the main cables over the two side spans could be different. Compared with the time-domain response, the frequency-domain response is more meaningful to investigate the effect due to seismic loading. In the Wenchuan Earthquake event, it is difficult to find the change of the responses at the deck, main cables and anchorage before, during and after the earthquake in the time domain. In the frequency domain, however, there is an obvious increase of the response components in the frequency range less than 1.0 Hz during the earthquake. In particular, the spectral components at 0-0.4 Hz measured at the anchorage during the earthquake are much higher than those before and after the earthquake. This is attributed to the seismic loading with low-frequency components. In summary, the long-distance earthquake generates low-frequency excitation while this is not obvious for the middle- and short-distance earthquakes.

The Fast Bayesian FFT method is found to be applicable to identify the modal parameters of the full-scale bridge efficiently and accurately. The PSD of modal force in Mode L1 increases after the earthquake in the Wenchuan Earthquake while there is only a slight change for this quantity in other two earthquake events. It is believed that the increase is attributed to the long distance earthquake effect. After the Wenchuan Earthquake, the identified damping ratios decrease for almost all the modes in the vertical direction. This is not observed in the lateral modes and other earthquake events. This may be also due to the earthquake effect.

One important merit of the Bayesian approach is that it is not only able to identify the most probable value of the modal parameters but also to obtain the posterior uncertainty of these parameters identified. The COVs of the modal frequencies are in the order of less than 1%, while the COVs of the damping ratios and PSDs of modal force are in the order of several tens percent. In the course of the Wenchuan Earthquake, the COVs of natural frequencies for the vertical modes tend to decrease while the COVs of the damping ratios tend to increase. This trend cannot be found in the lateral modes and other two earthquake events. The detail reason is still under investigation.

Acknowledgements

The work described in this paper was supported in part by a grant from The Hong Kong Polytechnic University under Grant No. 4-ZZCE and partially by a grant from the Research Grants Council of the Hong Kong Special Administrative Region, China (Project No. PolyU 5224/13E). These supports are greatly acknowledged.

References

Arici, Y. and Mosalam, K.M. (2003), “System identification of instrumented bridge systems”, *Earthq. Eng.*

Struct. Dyn., **32**(7), 999-1020.

Au, S.K. (2011), "Fast Bayesian FFT method for ambient modal identification with separated modes", *J. Eng. Mech.*, ASCE, **137**(3), 214-226.

Au, S.K. (2012a), "Fast Bayesian ambient modal identification in the frequency domain, Part I: Posterior most probable value", *Mech. Syst. Signal Pr.*, **26**, 60-75.

Au, S.K. (2012b), "Fast Bayesian ambient modal identification in the frequency domain, Part II: posterior uncertainty", *Mech. Syst. Signal Pr.*, **26**, 76-90.

Au, S.K. and Zhang, F.L. (2011), "On assessing the posterior mode shape uncertainty in ambient modal identification", *Prob. Eng. Mech.*, **26**(3), 427-434.

Au, S.K., Zhang, F.L. and Ni, Y.C. (2013), "Bayesian operational modal analysis: theory, computation, practice", *Comput. Struct.*, **126**, 3-15.

Beck, J.L. (2010), "Bayesian system identification based on probability logic", *Struct. Control Hlth. Monit.*, **17**(7), 825-847.

Beck, J.L. and Jennings, P.C. (1980), "Structural identification using linear model and earthquake records", *Earthq. Eng. Struct. Dyn.*, **8**(2), 145-160

Brownjohn, J.M.W., Moyo, P., Omenzetter, P. and Chakraborty, S. (2005), "Lessons from monitoring the performance of highway bridge", *Struct. Control Hlth. Monit.*, **12**(3-4), 227-244.

Casciati, S., Tento, A., Marcellini, A. and Daminell, R. (2014), "*Long run ambient noise recording for a masonry medieval tower*", *Smart Struct. Syst.*, **14**(3), 367-376.

China Earthquake Network Center. http://www.csndmc.ac.cn/newweb/index.jsp

Gomez, H.C., Ulusoy, H.S. and Feng, M.Q. (2013), "Variation of modal parameters of a highway bridge extracted from six earthquake records", *Earthq. Eng. Struct. Dyn.*, **42**(4), 565-579.

Hong Kong Observatory. http://www.weather.gov.hk/contente.htm

Ivanovic, S.S., Trifunac, M.D. and Todorovska, M.I. (2000), "Ambient vibration tests of structures-a review", *J. Earthq. Technol.*, ISET, **37**(4), 165-197.

Ko, J.M. and Ni, Y.Q. (2005), "Technology developments in structural health monitoring of large-scale bridges", *Eng. Struct.*, **27**(12), 1715-1725.

Loh, C.H. and Lee, Z.K. (1997), "Seismic monitoring of a bridge: assessing dynamic characteristics from both weak and strong ground excitations", *Earthq. Eng. Struct. Dyn.*, **26**(2), 269-288.

Loh, C.H. and Lin, H.M. (1996), "Application of off-line and on-line identification techniques to building seismic response data", *Earthq. Eng. Struct. Dyn.*, **25**(3), 269-290.

Michel, C., Gueguen, P., El Arem, S., Mazars, J. and Kotronis, P. (2010), "Full-scale dynamic response of a RC building under weak seismic motions using earthquake recordings, ambient vibrations and modeling", *Earthq. Eng. Struct. Dyn.*, **39**(4), 419-441.

Ni, Y.Q., Hua, X.G., Fan, K.Q. and Ko, J.M. (2005), "Correlating modal properties with temperature using long-term monitoring data and support vector machine techniques", *Eng. Struct.*, **27**(12), 1762-1773.

Ni, Y.Q., Wang, J.Y. and Ko, J.M. (1999), "Finite element modelling and modal sensitivity analysis of the Tsing Ma Suspension Bridge", Report No. WASHMS-03(a), Department of Civil and Structural Engineering, Hong Kong Polytechnic University, Hong Kong.

Ni, Y.Q., Wong, K.Y. and Xia, Y. (2011), "Health checks through landmark bridges to sky-high structures", *Adv. Struct. Eng.*, **14**(1), 103-119.

Ni, Y.Q., Xia, Y., Liao, W.Y. and Ko, J.M. (2009), "Technology innovation in developing the structural health monitoring system for Guangzhou New TV Tower", *Struct. Control Hlth. Monit.*, **16**(1), 73-98.

Ou, J. and Li, H. (2009), "Structural health monitoring research in China: trends and applications", *Struct. Health Monit. Civ. Infrastruct. Syst.*, Eds. V.M. Karbhari and F. Ansari, Woodhead Publishing, Cambridge, UK.

Papadimitriou, C., Beck, J.L. and Katafygiotis, L.S. (2001), "Updating robust reliability using structural test data", *Prob. Eng. Mech.*, **16**(2), 103-113.

Siringoringo, D.M. and Fujino, Y. (2006), "Observed dynamic performance of the Yokohama-Bay Bridge from system identification using seismic records", *Struct. Control Hlth. Monit.*, **13**(1), 226-244.

Smyth, A.W., Pei, J.S. and Masri, S.F. (2003), "System identification of the Vincent Thomas suspension

bridge using earthquake records", *Earthq. Eng. Struct. Dyn.*, **32**(3), 339-367.
Todorovska, M.I. and Trifunac, M.D. (2008), "Impulse response analysis of the VanNuys 7-story hotel during 11 earthquakes and earthquake damage detection", *Struct. Control Hlth. Monit.*, **15**(1), 90-116.
Ulusoy, H.S., Feng, M.Q. and Fanning, P.J. (2011), "System identification of a building from multiple seismic records", *Earthq. Eng. Struct. Dyn.*, **40**(6), 661-674.
Wang, J.Y., Ko, J.M. and Ni, Y.Q. (2000), "Modal sensitivity analysis of Tsing Ma Bridge for structural damage detection", *Nondestructive Evaluation of Highways, Utilities, and Pipelines IV*, Eds. A.E. Aktan and S.R. Gosselin, SPIE, **3995**, 300-311.
Wong, K.Y. (2004), "Instrumentation and health monitoring of cable-supported bridges", *Struct. Control Hlth. Monit.*, **11**(2), 91-124.
Wong, K.Y. and Ni, Y.Q. (2011), "Structural health monitoring of a suspension bridge", *Monitoring Technologies for Bridge Management*, Eds. B. Bakht, A.A. Mufti and L.D. Wegner, Multi-Science Publishing, Essex, UK.
Xia, Y., Hao, H., Zanardo, G. and Deeks, A. (2006), "Long term vibration monitoring of an RC slab: temperature and humidity effect", *Eng. Struct.*, **28**(3), 441-452.
Yuen, K.V. and Katafygiotis, L.S. (2003), "Bayesian fast Fourier transform approach for modal updating using ambient data", *Adv. Struct. Eng.*, **6**(2), 81-95.
Yuen, K.V. and Kuok, S.C. (2010), "Ambient interference in long-term monitoring of buildings", *Eng. Struct.*, **32**(8), 2379-2386.
Zhang, F.L. and Au, S.K. (2013), "Erratum for Fast Bayesian FFT method for ambient modal identification with separated modes by Siu-Kui Au", *J. Eng. Mech.*, ASCE, **139**(4), 545-545.

CN